THEORY AND EXPERIMENTS ON THE COMPLIANCE CONTROL OF REDUNDANT MANIPULATORS

H. Kazerooni, K. G. Bouklas, and J. Guo
Mechanical Engineering Department
University of Minnesota
Minneapolis, Minnesota

ABSTRACT

This work presents a control methodology for compliant motion in redundant robot manipulators. This control approach takes advantage of the redundancy in the robot's degrees of freedom: while a maximum six degrees of freedom of the robot control the robot's endpoint position, the remaining degrees of freedom impose an appropriate force on the environment. To verify the applicability of this control method, an active end-effector is mounted on an industrial robot to generate redundancy in the degrees of freedom. A set of experiments are described to demonstrate the use of this control method in constrained maneuvers. The stability of the robot and the environment is analyzed.

1. INTRODUCTION

Robotic manipulations fall into two categories: unconstrained and constrained maneuvers [3,4]. In unconstrained maneuvers, the robot moves freely in its workspace without contacting the environment. In constrained maneuvers, such as robotic deburring [7], the robot moves in its workspace in such a way that the environment continuously exerts a dynamic or kinematic constraint on the robot motion. If a position controller is used in constrained maneuvers, the robot-environment interaction forces are treated as disturbances and the controller rejects them, thus causing more interaction forces. The consequences of this type of interaction are saturation, instability and physical failure. Therefore the interaction forces in constrained maneuvers must be accommodated rather than resisted. Various methodologies for development of compliant motion exist where the measurement and feedback of the contact force is of paramount importance [9-14]. Reference 14 gives a thorough review and comparison of these methodologies.

The manipulator is assumed to have two mechanical parts: the primary manipulator and the secondary manipulator. The primary manipulator is used solely as a positioning system. The secondary manipulator, mounted on the endpoint of the primary manipulator, imposes a desired force on the environment (Figure 1). Even though the secondary manipulator holds the tool, it is not meant to be used for maneuvering objects. In fact, the goal is to use the secondary manipulator at a particular and fixed configuration relative to the last link of the primary manipulator. Figure 2 shows several configurations of the primary robot where the secondary manipulator has a fixed orientation. If the joints of the secondary manipulator are mechanically locked, the secondary manipulator can be considered to be a rigid body connected to the last link of the primary manipulator. If a regulator controller is placed on each joint of the secondary manipulator, the compliance of the secondary manipulator can be governed by adjusting the loop gains on the servo motors. If the loop gains on the servo motors are small, the system exhibits compliancy in response to forces imposed at its endpoint. If the loop gains are large, the secondary manipulator is very stiff electronically.

This paper describes a stable control method for development of compliant motion on the secondary manipulator. Sections 2 and 3 describe the unstructured dynamic model of the system. Sections 4 and 5 are dedicated to the control and stability criterion. Section 6 proves the integrity of the control approach via a set of experiments.

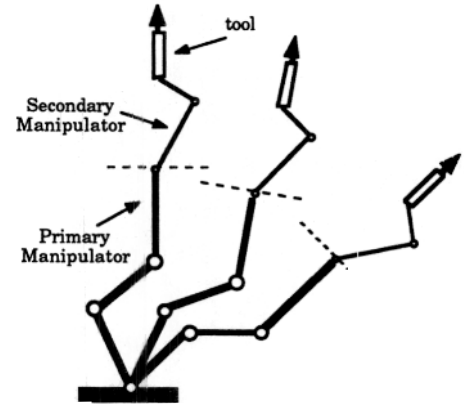

Figure 1: Various configurations of the primary manipulator where the secondary manipulator has a fixed orientation relative to its base

2. UNSTRUCTURED MODELING OF THE SECONDARY MANIPULATOR

The primary manipulator is assumed to have a trajectory controller for positioning its endpoint (i.e. the base of the secondary manipulator). Several linear and nonlinear control methods can be used to develop this trajectory controller. However, the concern here is the control and modeling of the secondary manipulator. The secondary manipulator motors are assumed to have velocity controllers since most servo motors have rate controllers. In general, a robotic system with a velocity controller has a velocity that is a dynamic function of its input vector[1], e, and of the force, d, imposed at its endpoint. The velocity controller for the secondary manipulator is assumed to have zero velocity input in the neighborhood of a particular configuration of the active end-effector. Thus, the active end-effector is not used for maneuvering parts, but is used at a particular known configuration. Therefore, the dynamic behavior of the secondary manipulator is expressed in terms of linear transfer function matrices, not to simplify the problem, but because of the nature of end-effector operation. Let G and S_0 be two

[1] The input commands to the secondary manipulator can be a set of voltages to the amplifiers, currents to the servo valves, or a set of numbers to the computer.

transfer function matrices that define the velocity deviation from zero of the secondary manipulator's endpoint.

$$\dot{x}(j\omega) = G(j\omega)\, e(j\omega) + S_o(j\omega)\, d(j\omega) \qquad (1)$$

where:

- $\dot{x}$: $n \times 1$ velocity vector of the secondary manipulator's endpoint in a coordinate frame attached to the last link of the primary manipulator
- e: $n \times 1$ input velocity vector
- d: $n \times 1$ force vector acting on the endpoint
- G: closed-loop velocity transfer function matrix from the input velocity vector, e, to the endpoint velocity, $\dot{x}$
- S_o: closed-loop sensitivity transfer function matrix from forces, d, to the end point velocity, $\dot{x}$
- n: the degrees of freedom of the secondary manipulator.

The type of velocity controller used is not important at this stage. Generally, systems with velocity controllers are not infinitely stiff in response to imposed forces (disturbances), d. The motion of the secondary manipulator's endpoint in response to imposed forces is caused either by structural compliance in the secondary manipulator or by compliance in the velocity controller. For a "good" velocity controller, S_o is "small"[2]. Non-direct drive systems with large gear ratios develop "small" sensitivity to imposed forces.

3. DYNAMIC BEHAVIOR OF THE ENVIRONMENT

If one point on the environment surface is displaced as much as y, the force required for such a task is defined by f (Figure 2).

$$f(j\omega) = E(j\omega)\, y(j\omega) \qquad (2)$$

$E(j\omega)$ is a square transfer function matrix that maps the amplitude of the displacement vector, y, to the amplitude of the contact force, f. Validation of equation 2 can be achieved by analyzing the relationship of the force and displacement of a spring as a simple model of the environment. E is the spring stiffness. (Hereafter, the argument $(j\omega)$ is dropped.) The relevant directions of the environment dynamics are those that constrain the workspace of the secondary manipulator. Therefore, E is an $n \times n$ matrix. E is a singular matrix when the robot interacts with the environment only in some directions. For example, in sliding on a frictionless surface, the secondary manipulator is constrained by the environment only in the direction normal to the surface.

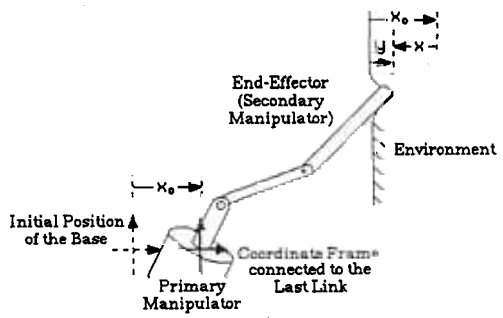

Figure 2: When the base of the secondary manipulator is moved as much as x_o, its endpoint moves as much as x relative to its base such that $y = x_o + x$.

4. THE ARCHITECTURE OF THE CLOSED-LOOP SYSTEM

Suppose the secondary manipulator, described by dynamic equation 1, is in contact with an environment given by equation 2. The block diagram of Figure 3 shows how the two systems interact when they are in contact. Note that $f = -d$. The secondary manipulator motion relative to its base (i.e. the last link of the primary manipulator) is represented by x. If the motion of the secondary manipulator base in a global Cartesian coordinate frame is characterized by a vector x_o then the absolute motion of the secondary manipulator endpoint, y, is $x_o + x$. When the secondary manipulator is in contact with the environment, the primary manipulator must not be maneuvered along those directions in which the secondary manipulator has no degrees of freedom. Thus, the vector x_o must be in the workspace of the secondary manipulator and is an $n \times 1$ vector.

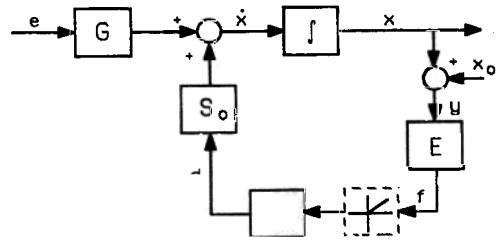

Figure 3: Dynamic Behavior of the Secondary Manipulator in Contact with the Environment. The Laplace operators of the transfer functions have been eliminated in all the block diagrams.

Figure 4 shows the proposed closed-loop control architecture for producing secondary manipulator compliancy[3]. The position deviation of the secondary manipulator is fed back to the system via the compensator K_p, a transfer function matrix that operates on the endpoint position. This creates a regulator controller for the secondary manipulator around its nominal configuration. This system has an "inner" loop and an "outer" loop. The "inner" loop is the "natural" feedback between the contact force and the environment. The "outer" loop is the controlled feedback. When the secondary manipulator is not in contact with the environment, the closed-loop system reduces to the "outer" loop. This is a simple closed-loop positioning system with an input position command equal to zero.

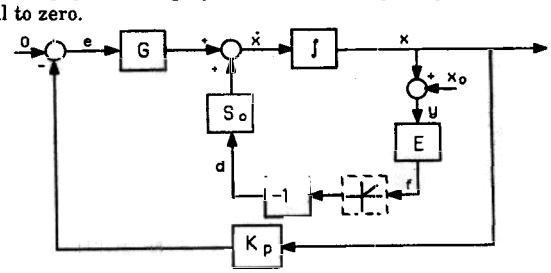

Figure 4: The Closed-loop Architecture

If the secondary manipulator's base is moved by x_o and the secondary manipulator encounters the environment (see Figure 2), the contact force can be computed from equation 3.

$$f = [\, I + E\,(s\, I + G\, K_p)^{-1}\, S_o]^{-1}\, E\, x_o \qquad (3)$$

In most manipulation tasks such as deburring or grinding, the robot manipulator contacts very stiff environments where E is "large". When E approaches infinity in the singular value sense, the interaction force between the secondary manipulator's endpoint and the environment is given by equation 4.

---

[2] "Small" means that the maximum singular value of the matrix is a small number. This concept can be extended to express the "large" size of a matrix using its minimum singular value. See footnote 4 for a definition on singular values.

[3] In some applications, the endpoint will only apply a unidirectional force to the environment. For example, in robotic grinding, the manipulator can only push the tool into the surface. If we consider a positive f_i for "pushing" and a negative f_i for "pulling", the active end-effector and the environment are then in contact with each other along those directions where $f_i > 0$ for $i=1,\ldots,n$. On the other hand, in some applications such as screwing in a bolt, the interaction force can be positive and negative. This means that the active end-effector can have clockwise and counterclockwise interaction torque. The nonlinear discriminator block diagram in Figure 3 is drawn with a dashed line to illustrate the above concept. Note the natural feedback in the system; the force developed in the system due to the interaction of the active end-effector and the environment affects the active end-effector motion in a feedback fashion.

$$f = S_o^{-1}(sI + G K_p) x_o \qquad (4)$$

This equation calculates the contact force on the environment when the secondary manipulator base moves towards the environment as much as x_o. Given G and S_o over a particular frequency range, a compensator K_p can be found to arbitrarily shape the system impedance, $S_o^{-1}(sI + G K_p)$. Under DC conditions where s= 0 and G= I, the stiffness of the system is expressed by equation 5:

$$f = S_o^{-1} K_p(0) x_o \qquad (5)$$

where x_o is the base position determined by the position of the primary manipulator. When K_p is a transfer function with a large magnitude in a particular direction, the contact force is large in that direction, while a small value for K_p leads to a small force.

5. STABILITY

In this section, a sufficient stability condition is given for the closed-loop system shown in Figure 4. By satisfying this condition, the designer can select the appropriate compensator K_p which guarantees system stability and develops compliancy as defined by either equality 3 or 4. The Multivariable Nyquist Criterion is used to derive the stability condition in Appendix A. The sufficient condition for stability is given by inequality 6:

$$\sigma_{max}(GK_p) < \sigma_{min}(sI + S_oE) \qquad \text{for all } \omega\in(0,\infty) \qquad (6)$$

or by a more conservative condition in inequality 7:

$$\sigma_{max}(K_p) < \frac{1}{\sigma_{max}(G)\sigma_{max}(sI + S_oE)^{-1}} \qquad \text{for all } \omega\in(0,\infty) \qquad (7)$$

where σ_{max} indicates the maximum singular value[4] of a matrix. The above condition guarantees stability of the robot when it is in contact with the environment. If the compensator K_p does not satisfy this condition, no conclusion can be made about the system stability. When n=1, the sufficient condition for stability is given by inequality 8.

$$|GK_p| < |s + S_oE| \qquad \text{for all } \omega\in(0,\infty) \qquad (8)$$

Since G≈1 within $(0,\omega_o)$, where ω_o is the velocity controller bandwidth, the sufficient condition is:

$$|K_p| < |s + S_oE| \qquad \text{for all } \omega\in(0,\omega_o) \qquad (9)$$

One important class of manipulations places the robot in contact with a very rigid environment. Equations 7, 8, and 9 show that the system is always stable if E is very "large" in the singular value sense and $S_o \neq 0$. In this case, the gain of the feedback compensator K_p can be chosen to be large enough to guarantee stability. Note that, in practice, K_p cannot be chosen as an integrator because an integrator has an infinite magnitude at DC which leads to saturation and unboundedness of the contact force when an infinitely rigid constraint is imposed on a servo system.

When the environment is infinitely rigid, a large stability range gives the designer freedom to shape the force function without being confined by the stability condition. This is the advantage of this compliance control method in comparison with methods that use force sensors.

6. AN EXPERIMENTAL PROTOTYPE ACTIVE END-EFFECTOR AND ITS DYNAMIC MODEL

To verify the applicability of this control method, a two-degree-of-freedom active end-effector is mounted on an industrial robot as the secondary manipulator to generate redundancy in the robot's degrees of freedom. Several experiments are presented to verify the theory developed in the previous sections. The device utilized for these experiments is a planar, five-bar linkage [5] which is driven by two direct drive, brushless DC motors (Moog Inc., Model 303-002). Both of the active end-effector motors are fixed to the last link of the primary manipulator (Figure 5). Two PWM amplifiers (Moog Inc., 152-200 Series) interface the motors to the analog velocity controllers. An IBM/AT microcomputer is the main controller providing the compensator K_p.

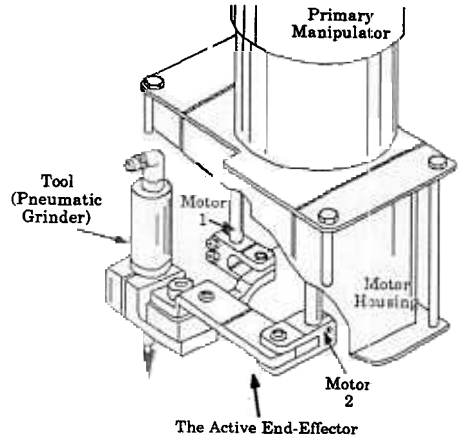

Figure 5: The Active End-Effector

Figure 6 shows the active end-effector mechanism where the endpoint can be moved in a planar space via two motors. The end-effector operates in the neighborhood of the configuration shown in Figure 6, where all the links are orthogonal to each other. In this configuration, both the Inertia matrix and the Jacobian matrix are constant and diagonal [1]. This leads to an uncoupled dynamic equation for the active end-effector at its nominal configuration, enabling motor 1 to move the endpoint in the x_1 direction and motor 2 to move the endpoint in the x_2 direction.

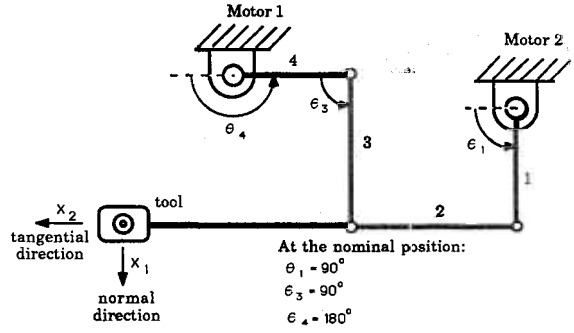

Figure 6: The Active End-Effector at its Nominal Position

The control analysis in previous sections requires a velocity controller as the lowest level of control. Since the dynamic behavior of the active end-effector is uncoupled in its nominal configuration, separate control loops are needed for each motor. Motor 1 drives the endpoint in the normal direction while motor 2 drives the endpoint in the tangential direction. The Jacobian matrix relating the small perturbations of θ_1 and θ_2 to the perturbations of x_1 and x_2 is given by the following equation [5].

$$J = \begin{bmatrix} -1.768 & 0 \\ 0 & -0.906 \end{bmatrix} \qquad (10)$$

Using engineering data (inductance and resistance, shaft and links moments of inertia, and torque constants for the servo motors [2]), the theoretical closed-loop transfer function for each motor is derived in equations 11 and 12. The choice of compensators in the development of the closed-loop velocity controller is not of importance in this analysis. However, these compensators are designed so that the output velocity follows the input command as fast as possible while

[4] The maximum singular value of a matrix K_p, σ_{max} is defined as:

$$\sigma_{max}(K_p) = \max \frac{|K_p Z|}{|Z|}$$

where Z is a non-zero vector and |.| denotes the Euclidean norm.

the system remains stable in the presence of all unmodeled dynamics. These transfer functions are called $G'_1(s)$ and $G'_2(s)$ because they are calculated and measured in the joint angle space. Using the Jacobian in equation 10 results in equations 11 and 12 which present the closed-loop velocity in the global coordinate frame.

$$G'_1(s) = \frac{V_{out1}}{V_{in1}} = 0.818 \frac{(\frac{s}{6.66}+1)}{(\frac{s}{964.28}+1)(\frac{s}{3.103}+1)(\frac{s^2}{209089.8}+\frac{s}{351.34}+1)} \quad \left(\frac{\text{Volts}}{\text{Volts}}\right) \quad (11)$$

$$G'_2(s) = \frac{V_{out2}}{V_{in2}} = 1.346 \frac{(\frac{s}{6.66}+1)}{(\frac{s}{936}+1)(\frac{s}{3.88}+1)(\frac{s^2}{182373.23}+\frac{s}{324.87}+1)} \quad \left(\frac{\text{Volts}}{\text{Volts}}\right) \quad (12)$$

Where:

V_{in1} and V_{in2} : the input velocity command for each motor shaft in Volts

V_{out1} and V_{out2}: the output voltage representing the angular velocity of each motor shaft. One volt of tachometer output represents 0.0191 rad/sec of the shaft angular velocity.

The closed-loop transfer functions 11 and 12 are verified experimentally in the frequency domain. Figures 7 and 9 show the theoretical and experimental Bode plots of the closed-loop velocity transfer functions for both motors.

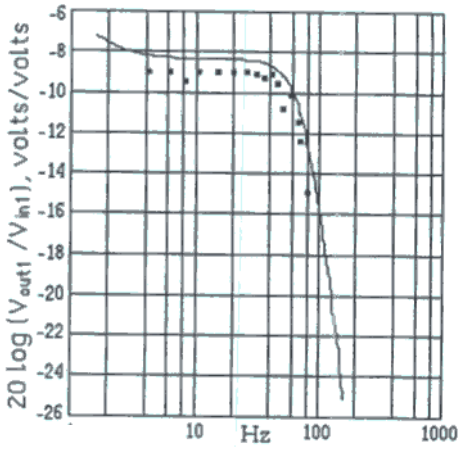

Figure 7: The Experiment and Simulation of the First Motor's Closed-loop Velocity Transfer Function, $G'_1(s)$.

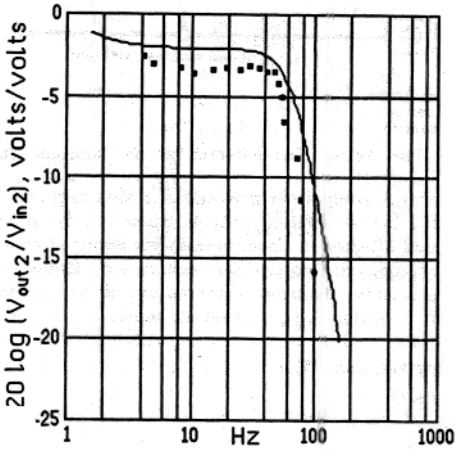

Figure 8: The Experiment and Simulation of the Second Motor's Closed-loop Velocity Transfer Function, $G'_2(s)$.

The theoretical sensitivity transfer functions for motors 1 and 2 are derived in equations 13 and 14 using the data from the engineering drawings. The notations $S'_{o1}(s)$ and $S'_{o2}(s)$ represent the sensitivity in the joint coordinate frame as opposed to $S_{o1}(s)$ and $S_{o2}(s)$ in the global Cartesian coordinate frame. Later, the Jacobian of equation 10 will be used to arrive at the sensitivity functions in the global coordinate frame.

$$S'_{o1}(s) = \frac{\dot{\theta}_1}{T_1} = \frac{1.775(\frac{s}{25}+1)(\frac{s}{0.9}+1)}{(\frac{s}{964.28}+1)(\frac{s}{3.103}+1)(\frac{s^2}{589.72}+\frac{s}{23.59}+1)} \quad \left(\frac{\text{rad sec}^{-1}}{\text{lbf in}}\right) \quad (13)$$

$$S'_{o2}(s) = \frac{\dot{\theta}_2}{T_2} = \frac{3.984(\frac{s}{43.3}+1)(\frac{s}{2}+1)}{(\frac{s}{936}+1)(\frac{s}{3.879}+1)(\frac{s^2}{2246.56}+\frac{s}{52}+1)} \quad \left(\frac{\text{rad sec}^{-1}}{\text{lbf in}}\right) \quad (14)$$

where:

$S'_{o1}(s)$ and $S'_{o2}(s)$: closed-loop sensitivity transfer functions from the external torque, T_1, and, T_2 to the angular velocity, $\dot{\theta}_1$ and $\dot{\theta}_2$.

$\dot{\theta}_1$ and $\dot{\theta}_2$: the velocity developed on the ith motor

T_1 and T_2: the external torque applied on the ith motor shaft.

To verify experimentally the sensitivity of the closed-loop velocity control system to external torques (equations 13 and 14), the apparatus in Figure 9 is used. An eccentric mass is mounted on the tool bit. The input excitation is supplied by the rotation of this mass. The rotation of the mass generates a sinusoidal torque disturbance at the corresponding motor shaft with a frequency equal to the frequency of the rotation of the mass. Figures 10 and 11 show the Bode plots of the theoretical and experimental sensitivity transfer functions.

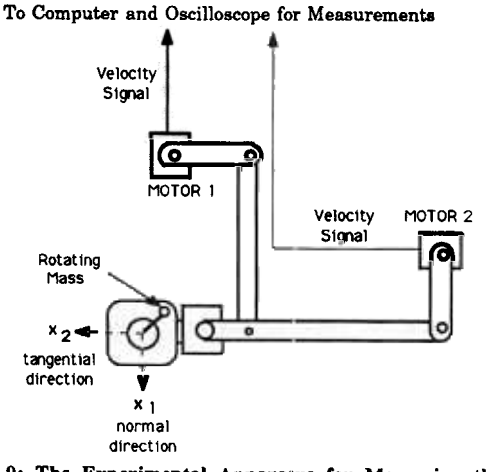

Figure 9: The Experimental Apparatus for Measuring the Sensitivity Transfer Function

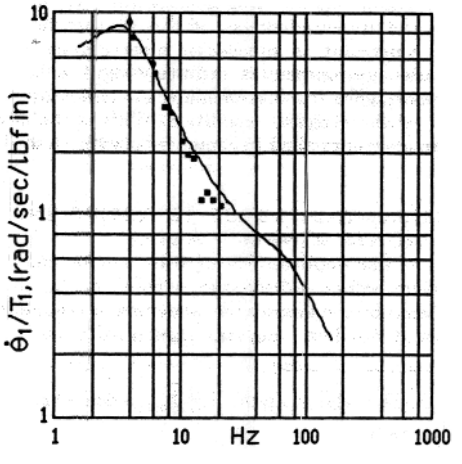

Figure 10: Sensitivity Transfer Function for Motor 1, $S'_{o1}(s)$.

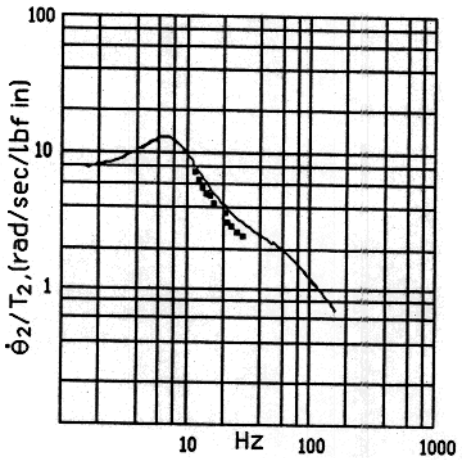

Figure 11: Sensitivity Transfer Function for Motor 2, $S'_{o2}(s)$.

7. COMPENSATOR DESIGN

After the closed-loop velocity transfer functions and the sensitivity transfer functions are determined, the position compensators, K_{p1} and K_{p2}, for each motor are designed. Since the active end-effector is used with a very hard environment, the system is stable for a wide selection of K_{p1} and K_{p2}, in accordance with the results given in section 5. K_{p1} and K_{p2} are chosen using equations 15 and 16.

$$K_{p1}(s) = 30 \frac{\frac{s}{1.5}+1}{\frac{s}{4.3}+1} \qquad (15)$$

$$K_{p2}(s) = 50.2 \frac{\frac{s}{3.5}+1}{\frac{s}{6}+1} \qquad (16)$$

The choice of K_{p1} and K_{p2} depends on the desired system impedance as defined in equation 4. The selection of a specific K_{p1} and K_{p2} enables the designer to shape the magnitude and bandwidth of the active end-effector impedance. The transfer functions in equations 15 and 16, for example, yield a flat impedance (equation 4) for a wide frequency range.

When the base of the active end-effector is moved by x_o towards the environment in the global coordinate frame, the contact forces (equation 4), are equal to that given by equation 17 :

$$f_1 = \frac{s + G_1K_{p1}}{S_{o1}} x_{o1} \quad \text{and} \quad f_2 = \frac{s + G_2K_{p2}}{S_{o2}} x_{o2} \qquad (17)$$

Note that x_{o1} and x_{o2} are the inputs to the system and the contact forces, f_1 and f_2, applied on the environment by the active end-effector are the outputs of the system. By assigning different position commands to the base of the active end-effector and by maintaining complete control on K_{p1} and K_{p2} in equation 17, a designer can keep the contact forces in a desired range. Also note that the active end-effector behaves like a system that accepts a set of positions as inputs and reflects a set of forces as output. This is a fundamental characteristic of impedance control which differentiates it from admittance control. Equation 17 will be verified experimentally in both directions. The frequency response experiment must be carried out by imposing sinosoidal input positions on the end-effector when it is in contact with a rigid wall. This requires the precise position of the active end-effector base, x_{o1} and x_{o2}. However, it is possible to verify equation 17 with a more convenient method when the active end-effector is not in contact with any environment.

When the active end-effector is not in contact with its environment, the relationship between the external force, d, and the endpoint position of the active end-effector, x, in the global Cartesian coordinate frame is given by equation 18. (This is the closed-loop positioning controller sensitivity.)

$$x = (sI + G K_p)^{-1} S_o d \qquad (18)$$

Since the active end-effector is dynamically uncoupled around its nominal position, equation 18 (in each direction) becomes:

$$x_1 = \frac{S_{o1}}{s + G_1K_{p1}} d_1 \qquad x_2 = \frac{S_{o2}}{s + G_2K_{p2}} d_2 \qquad (19)$$

where:

d_1 and d_2: the input excitation force applied at the endpoint of the active end- effector along the x_1 and x_2 directions. (lbf)

x_1 and x_2: the translational displacement of the active end-effector's endpoint from its nominal position.(in)

Comparing equations 17 and 19 reveals that, for measuring $\frac{s + G_1K_{p1}}{S_{o1}}$ and $\frac{s + G_2K_{p2}}{S_{o2}}$ (given by equation 17), one can use the same experimental set-up (Figure 10) employed to measure the closed-loop sensitivity, $\frac{S_{o1}}{s + G_1K_{p1}}$ and $\frac{S_{o2}}{s + G_2K_{p2}}$ (given by equation 19). In other words, the closed-loop system sensitivity in response to external forces (equation 19) is measured rather than measuring the system impedance in constrained maneuvers (equation 17). In general, for linear systems, the impedance function is equal to the inverse of the sensitivity function. For the experimental set-up (Figure 12), the following transfer functions give the sensitivity of each motor:

$$\frac{\theta_1}{T_1} = \frac{S'_{o1}(s)}{s + G_1(s)K_{p1}(s)} \text{ and } \frac{\theta_2}{T_2} = \frac{S'_{o2}(s)}{s + G_2(s)K_{p2}(s)} \left(\frac{\text{rad}}{\text{lbf in}}\right) (20)$$

where θ_1 and θ_2 are the small angular perturbations of the motor shafts in the neighborhood of their nominal positions and T_1 and T_2 are the imposed torques at each motor shaft. Using the Jacobian (equation 10) results in the following equations:

$$\frac{x_1}{d_1} = (-1.768)^2 \frac{\theta_1}{T_1} = (-1.768)^2 \frac{S'_{o1}(s)}{(s + G_1(s)K_{p1}(s))} \left(\frac{\text{in}}{\text{lbf}}\right) (21)$$

$$\frac{x_2}{d_2} = (-0.906)^2 \frac{\theta_2}{T_2} = (-0.906)^2 \frac{S'_{o2}(s)}{(s + G_2(s)K_{p2}(s))} \left(\frac{\text{in}}{\text{lbf}}\right) (22)$$

where d_1 and d_2 are the forces applied at the active end-effector's endpoint. An experiment is run to measure the active end-effector's endpoint sensitivity (equations 21 and 22.) The known or available quantities for measurement are: i) the excitation force (the centrifugal force due to rotating) and ii) the angular position of the motor shaft which is eventually converted into the active end-effector's endpoint displacement. The experimental data and the theoretical simulation of the endpoint sensitivity are presented in figures 12 and 13. With the appropriate selection of $K_{p1}(s)$ and $K_{p2}(s)$, the designer can shape the magnitude and bandwidth of the desired target impedance. The plots in Figures 12 and 13 show that the sensitivity in the normal direction (x_1) is larger than the sensitivity in the tangential direction (x_2). However, the architecture of the active end-effector in Figure 8 shows that the system naturally has a larger inertia (and consequently, smaller pen-loop sensitivity) in the x_1 direction. This shows that one can shape the impedance of the system arbitrarily so the system, in the closed-loop form, has an impedance dramatically different from its natural open-loop impedance. The strength of this alteration in the impedance magnitude and bandwidth is limited by the unmodeled dynamics in the system [4].

SUMMARY AND CONCLUSION

This paper describes a control method for development of compliant motion without using any force sensors. This control method benefits from redundancy in the robot degrees of freedom: the extra degrees of freedom in a particular robotic system can impose forces on the environment. The stability of the system and the environment is studied and a sufficient condition for stability is derived.

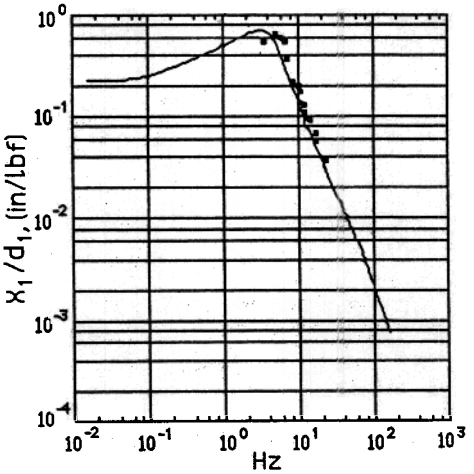

Figure 12: Endpoint Sensitivity (1/Impedance) in the Normal Direction (First Motor)

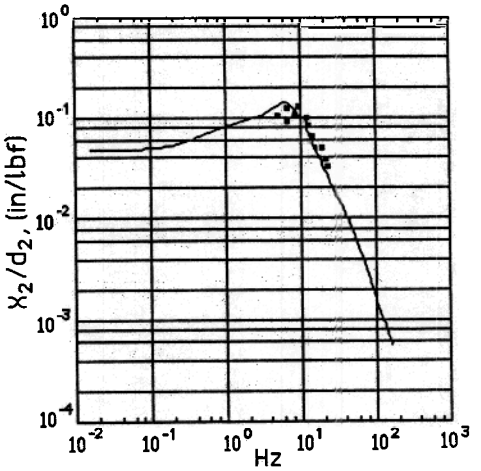

Figure 13: Endpoint Sensitivity (1/Impedance) in the Tangential Direction (Second Motor)

APPENDIX A

The objective here is to find a sufficient condition for the stability of the closed-loop system shown in Figure 6 by using the Multivariable Nyquist Criterion [8]. Equation A1 can be derived from Figure 6:

$$x = -(sI + S_oE + GK_p)^{-1} S_o E \, x_o \qquad \text{(A1)}$$

If $K_p = 0$, the block diagram shown in Figure A1 reduces to the system in Figure 5, which is a stable velocity-controlled active end-effector in contact with its environment.

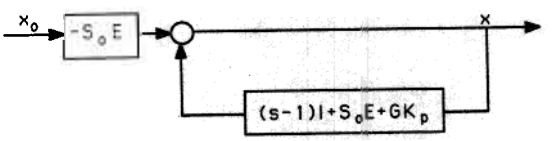

Figure A1: Modified Block Diagram of the Closed-loop Control System.

Assume the following conditions are satisfied:

1) The closed-loop system in Figure A1 is stable if $K_p=0$. This condition simply states the stability of the system in Figure 5.

2) K_p is a stable linear transfer function matrix. This implies that the number of unstable poles of $(s-1)I + S_oE + GK_p$ should be equal to the number of unstable poles of $(s-1)I + S_oE$.

3) The number of poles on the $j\omega$ axis of loops $(s-1)I + S_oE + GK_p$ and $(s-1)I + S_oE$ are equal. This condition states that K_p should not have any pole on the $j\omega$ axis.

Since the system in Figure A1 is stable when $K_p=0$, deriving a sufficient condition for stability of the closed-loop system requires investigation of the influence of GK_p. According to the Nyquist Criterion, the system in Figure A1 remains stable if the clockwise encirclement of $\det(sI + S_oE + GK_p)$ around the center of the **s-plane** is equal to the number of unstable poles of the loop transfer function $(s-1)I + S_oE + GK_p$. Taking into account conditions 1, 2 and 3, for the stability of the closed-loop system, $\det(sI + S_oE + GK_p)$ must have the same number of encirclements around the center of s-plane that $\det(sI + S_oE)$ has. This is true because $\det(sI + S_oE + GK_p)$ and $\det(sI + S_oE)$ have the same number of unstable poles. A sufficient condition which guarantees the equality of the number of encirclements of $\det(sI + S_oE + GK_p)$ and $\det(sI + S_oE)$ is that the $\det(sI + S_oE + GK_p)$ does not pass through the origin of the **s-plane** for all possible non-zero finite values of K_p or:

$$\det(sI + S_oE + GK_p) \neq 0 \quad \text{for all } \omega \in [0,\infty) \qquad \text{(A2)}$$

A sufficient condition that guarantees the above inequality is:

$$\sigma_{max}(GK_p) < \sigma_{min}(sI + S_oE) \quad \text{for all } \omega \in [0,\infty) \qquad \text{(A3)}$$

or more conservatively:

$$\sigma_{max}(K_p) < \frac{1}{\sigma_{max}((sI + S_oE)^{-1}G)} \quad \text{for all } \omega \in [0,\infty) \qquad \text{(A4)}$$

and for systems with one degree of freedom (n=1), the sufficient condition for stability is given by:

$$|GK_p| < |s + S_oE| \quad \text{for all } \omega \in [0,\infty) \qquad \text{(A5)}$$

REFERENCES

[1] Craig, J., "Introduction to Robotics, Mechanics and Control", Addison-Wesley Publishing Co., 1986.

[2] "DC Motors, Speed Controls, Servo Systems", Electro-craft Corp., Fifth Edition, 1980.

[3] Hogan, N., "Impedance Control: An Approach to Manipulation", ASME Journal of Dynamic Systems, Measurement, and Control, Volume 107, Number 1, pp. 1-24, March 1985.

[4] Kazerooni, H., Sheridan, T. B., Houpt, P. K., "Fundamentals of Robust Compliant Motion for Robot Manipulators", IEEE Journal on Robotics and Automation, V2, N2, June 1986.

[5] Kazerooni, H., "Direct Drive Active Compliant End-Effector (Active RCC)", IEEE Journal of Robotics and Automation, Volume 4, Number 3, June 1988. .

[6] Kazerooni, H., Tsay, T. I., "Stability Criteria for Robot Compliant Maneuvers", IEEE Conference on Robotics and Automation, April 1988, Philadelphia, PA.

[7] Kazerooni, H., Her, M., G., "Robotic Deburring of parts with Unknown Geometry", American Control Conference, Atlanta, Georgia, June 1988.

[8] Lehtomaki, N. A., Sandell, N. R., Athans, M., "Robustness Results in Linear-Quadratic Gaussian Based Multivariable Control Designs", IEEE Transaction on Automatic Control AC-26(1):75-92, February, 1981.

[9] Mason, M. T., "Compliance and Force Control for Computer Controlled Manipulators", IEEE Transaction on Systems, Man, and Cybernetics SMC-11(6):418-432, June, 1981.

[10] Paul, R. P. C., Shimano, B., "Compliance and Control", In Proceedings of the Joint Automatic Control Conference, pages 694-699. San Francisco, 1976.

[11] Raibert, M. H., Craig, J. J., "Hybrid Position/Force Control of Manipulators", ASME Journal of Dynamic Systems, Measurement, and Control Volume 102, June 1981.

[12] Salisbury, K. J., "Active Stiffness Control of a Manipulator in Cartesian Coordinates", IEEE Conference on Decision and Control, Albuquerque, New Mexico, Dec. 1980.

[13] Whitney, D. E., "Force-Feedback Control of Manipulator Fine Motions", ASME Journal of Dynamic Systems, Measurements and Control, June 1977.

[14] Whitney, D., E., "Historical Perspective and State of the Art in Robot Force Control", IEEE. International Conference on Robotics and Automation, St. Louis, Missouri, 1985.

[15] Wu, C. H., Paul, R. P., "Manipulator Compliance Based on Joint Torque Control", IEEE Conference on Decision and Control, Albuquerque, New Mexico, Dec. 1980.